Journal of
Applied Crystallography

ISSN 0021-8898

Received 10 January 2006
Accepted 2 March 2006

Dedicated to Hartmut Fuess on the occasion of his 65th birthday.

Three-dimensional birefringence imaging with a microscope tilting-stage. I. Uniaxial crystals

L. A. Pajdzik and A. M. Glazer*

Physics Department, University of Oxford, Parks Road, Oxford OX1 3PU, UK. Correspondence e-mail: glazer@physics.ox.ac.uk

The development of a microscope tilting-stage suitable for use with birefringence imaging is described, thus enabling precise three-dimensional birefringence information of uniaxial crystals to be obtained. Equations have been derived for uniaxial crystals in any orientation. The technique enables precise values of the birefringence $\Delta n = n_e - n_o$ (difference between extraordinary and ordinary refractive index) and orientation of the optic axis to be obtained. The sign of the optical indicatrix may be unambiguously identified. The method is also able to obtain information on preferred orientation in a polycrystalline material. In addition to this, an unknown crystalline material may be identified, or at least classified within a specific group of crystalline materials.

1. Introduction

Measurement of optical linear birefringence has been one of the standard tools in the study of anisotropic properties of materials for nearly two centuries. Classically, birefringence is detected or measured using the crossed-polars technique, where the sample is placed between two polarizers that are oriented so that their planes of vibration are mutually perpendicular (see for example, Hartshorne & Stuart, 1964, 1970). When an isotropic sample is placed between crossed polars, the state of the polarization of light is unchanged and in theory no light is transmitted through the optical system. The light can only be transmitted if the state of polarization is changed, *i.e.* the sample is birefringent.

Consider plane-polarized light passing through a birefringent material. The light is then split into two rays travelling subject to different refractive indices n'' and n'. These refractive indices can be described by an ellipsoid known as the optical indicatrix with semi-axes n_e and n_o, the extraordinary and ordinary refractive indices, respectively. This introduces a phase difference between the two light paths so that when the two rays recombine, the final phase difference δ between them is a measure of the optical anisotropy of the birefringent material. The phase difference is given by

$$\delta = \frac{2\pi}{\lambda}(n'' - n')t, \tag{1}$$

where λ is the wavelength of the light, t is the thickness of the sample, and $n'' - n'$ is the so-called plano-birefringence of the sample. Strictly speaking, the 'birefringence', which is a characteristic of the sample, is obtained only when n'' and n' coincide with n_e and n_o.

The crossed-polars technique is fast and easy, but it has a number of disadvantages. If the birefringence of the sample is very low, it can be difficult to detect. Moreover, in this technique the sample must be oriented with respect to the polarization direction of the light. This makes the crossed-polars technique impractical for determination of birefringence in non-homogenous samples, because the sample needs to be rotated to compare different regions simultaneously. Because of this, some years ago we developed a new method for automatically recording birefringence by making use of a rotating polarizer and a circular analyzer attached to a microscope combined with a camera to image the field of view (Glazer *et al.*, 1996). This technique has subsequently been commercialized under the name Metripol (see http://www.metripol.com).

This system uses monochromatic light, a plane polarizer capable of being rotated to fixed angles α from a reference position, a circular-polarizing analyzer, a CCD camera, an electronic controller and computer software for polarizer control, image collection and analysis. Monochromatic light passes through the rotating polarizer and then through the birefringent sample (Fig. 1). The light from the sample then passes through a quarter-wave plate and analyzer (arranged together to form a circular analyzer) to provide an image which is captured by the CCD camera. The signal is transferred to a computer where it is processed by specially written software.

The intensity of the light I measured at any position within the image captured by the CCD camera is a function of the angular orientation α of the rotating polarizer and is defined by

$$I = \frac{I_0}{2}[1 + \sin(2\phi - 2\alpha)\sin\delta], \tag{2}$$

where I_0 is the intensity of unpolarized light transmitted through the sample and ϕ is the orientation angle of one of the

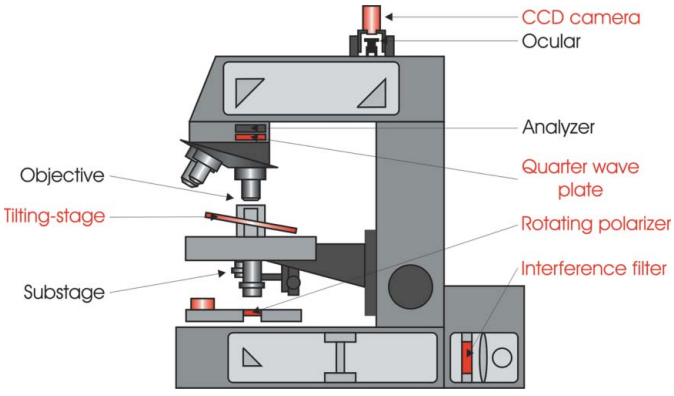

Figure 1
Metripol with a tilting-stage. The components that are additional to the polarizing microscope are highlighted in red.

axes of a section of the optical indicatrix measured from a predetermined direction (the so-called azimuthal angle[1]). The phase shift in this formula is then a measure of the effective birefringence projected onto the plane of the sample, *i.e.* the plano-birefringence.

By carrying out measurements of this intensity for several values of α, it is possible at each position in the digital image to use least squares to compute the quantities $|\sin\delta|$, ϕ and I_0 (Glazer *et al.*, 1996). Each of these three quantities can then be presented as a colour-coded image of the sample, thus separating out each of the components that are normally superimposed in a conventional crossed-polars image. The advantages of this method are obvious: the three quantities can be measured from all parts of the sample image simultaneously, the technique is capable of extremely high sensitivity, and in addition it does not depend on the orientation of the sample to a particular angle with respect to the polarization direction.

However, measurement of $|\sin\delta|$, carried out at a single wavelength with an ordinary microscope stage, does not provide any information concerning the number of periods of the $|\sin\delta|$ function, so that in general it is not possible to determine directly the actual value of the phase difference and thus the optical retardance and the birefringence of the sample. This also means that each time $|\sin\delta|$ passes through zero, the computed value of the azimuthal angle ϕ changes through 90°. In this case, the determination of the absolute value of the birefringence is limited to a relatively low phase difference δ, where

$$|\delta| = \sin^{-1}(|\sin\delta|) \quad \text{for} \quad |\delta| \leq \pi/2. \tag{3}$$

This ambiguity results from the fact that $m\pi$, where m is a positive integer, can be added to the measured relative phase difference δ_0 for positive slopes of the $|\sin\delta|$ function or to $-\delta_0$ for negative slopes of the $|\sin\delta|$ function, without change of $|\sin\delta|$ itself. This means that

$$|\delta| = \delta_0 + m\pi \quad \text{or} \quad |\delta| = -\delta_0 + m\pi \tag{4}$$

for positive and negative slopes of $|\sin\delta|$, respectively, and

$$\delta_0 = \sin^{-1}(|\sin\delta|). \tag{5}$$

In order to obtain the absolute values of the phase difference δ, a multiwavelength measurement may be carried out (Geday *et al.*, 2000). In this case the ambiguity may be solved from the derivative of the relative phase difference δ_0 with respect to the wavelength λ, expressed here using the wavevector length k:

$$\frac{\partial\delta_0}{\partial k} = \pm t\left[(n'' - n') + k\frac{\partial}{\partial k}(n'' - n')\right], \tag{6}$$

where

$$k = \frac{2\pi}{\lambda}. \tag{7}$$

The second term in equation (6) defines the dispersion of the double refraction. If this is small, this term may be neglected and equation (6) becomes

$$\delta_1 = \pm k_1\frac{\partial\delta_0}{\partial k} = k_1\lim_{k_2\to k_1}\left(\frac{\delta_{0,2} - \delta_{0,1}}{k_2 - k_1}\right), \tag{8}$$

where $\delta_{0,1}$ and $\delta_{0,2}$ are the values of the relative phase difference measured at two different wavelengths λ_1 and λ_2, respectively, and δ_1 is the absolute value of the phase difference calculated for the first chosen wavelength. The multiwavelength method, however, does exhibit a number of difficulties. Note that equation (8) cannot always be used to calculate the absolute value of phase difference δ_1 because $\delta_{0,1}$ and $\delta_{0,2}$ might not belong to the same slope of the $|\sin\delta|$ function. Moreover, the reliability of this method strongly depends on the precision in measuring $|\sin\delta|$ and the amount of optical dispersion of the double refraction in the case of birefringent materials with high optical dispersion. Note also that the multiwavelength method only provides information on the absolute values. We show below how our new method can obtain the actual value of the phase difference automatically, and thus the optical retardance and the birefringence, including its sign.[2]

The Metripol method has already been used for a broad range of applications, including phase transition studies (see for example, Geday *et al.*, 2000), mineral analysis, strain analysis, and location of defects through strain fields (see for example, Glazer *et al.*, 1996). More recent applications of the Metripol system also include the investigation of macroscopic symmetry of $Pb(Mg_{1/3}Nb_{2/3})_{1-x}Ti_xO_3$ in the morphotropic phase boundary region (Shuvaeva *et al.*, 2005), morphological and optical characteristics of nanocrystalline thin films (Ye *et al.*, 2006), stability of cellulose lyotropic liquid-crystal emulsions (Tixier *et al.*, 2005), and predetermination of the diffraction quality of protein crystals (Owen & Garman, 2005). Moreover, Hollingsworth & Peterson (2002) have applied the

[1] The value of the azimuthal angle ϕ is measured anticlockwise from the horizontal direction within the image captured by the CCD camera.

[2] The value of the birefringence, and thus the optical retardance and the phase difference, takes a positive value when the sign of the optical indicatrix is positive and a negative value when the sign of the optical indicatrix is negative.

Metripol technique in order to demonstrate domain switching in ferroelastic pseudo-hexagonal crystals of 2,10-undecanedione. In the present paper, we extend the technique in order to obtain automatically three-dimensional birefringence information from uniaxial crystals by adding a tilting-stage to the microscope (Fig. 1).

Examination of crystals using a polarizing microscope in the orthoscopic configuration and with an ordinary microscope stage reveals their optical character only in one direction. Much more additional optical information is obtained using a universal or tilting-stage which allows one to examine the optical properties of crystals in many directions. The idea of using tilting-stages goes back to the 19th century, where they were used in order to measure manually the birefringence out of the plane of the sample-stage. The method was complicated, lengthy and difficult, and as a result fell out of general use. However, with the technology available today, much of the early difficulty can be overcome through the use of computers and imaging devices.

More recently (Heilbronner, 2000), a tilting-stage has been used to obtain orientation images of crystals using polarization measurements on digital images with a look-up table. In order to obtain orientation images in this way, typically 18 rotation images, two or four tilt images and one circular polarization image are collected.

Below we present a method which is less complicated and automatically provides more information concerning the optical properties of birefringent crystals. To do this, we combine the idea of the tilting-stage with the advantages of the Metripol technique to give a new method for three-dimensional analysis of birefringent materials, which may have applications in the field of crystallography, mineralogy, archaeology, chemistry, biology, *etc*.

An important advantage is that the tilting-stage makes possible automatic identification of an unknown crystalline material or at least classification within a specific group of crystalline materials. Furthermore, for crystallites in polycrystalline materials, the method allows us to obtain precise information on preferred orientation. We show below how our method can obtain such texture information automatically.

2. Tilting-stage technique

Fig. 1 shows the addition of the tilting-stage to the sample-stage of a microscope, while Fig. 2 shows a schematic view of the tilting-stage.

The tilting-stage was constructed with two stepper motors, a set of gears and bevel bearings, two shafts and a metal frame. These parts together form a mechanical system which is capable of being tilted to specific angles Θ_1 and Θ_2 from a reference position about two orthogonal tilt axes. These have a maximum angular range of $\pm 12^\circ$ and a minimum angular step of 0.005° and 0.02°, respectively. The microscope stage is fully computer-controlled *via* the stepper motors. A computer program was written in Visual C++ in order to perform the actual measurement process and the subsequent analysis of the data was carried out using *MATLAB* (http://www.mathworks.com). This program was designed to interface with the Metripol software.

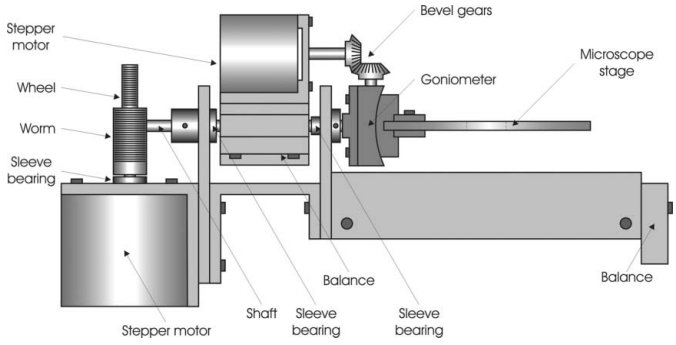

Figure 2
Schematic diagram of the tilting-stage.

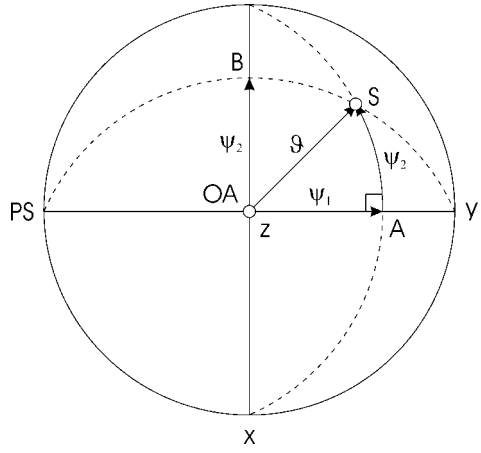

Figure 3
Stereographic representation of the optical indicatrix for a uniaxial sample. Note that ψ_2 is given by OA–*B* and is equal to the great circle angle *S*–*A*.

2.1. Derivation of formulae

Fig. 3 shows a stereographic representation of the optical indicatrix for a uniaxial sample. OA denotes the optic axis and PS denotes an arbitrarily chosen principal section of the optical indicatrix containing the optic axis OA. The x and y axes correspond to the directions of the ordinary refractive index n_o, and the z axis corresponds to the extraordinary refractive index n_e. We assume here that the z axis is perpendicular to the plane of the drawing. S denotes a general direction of propagation of the light within the sample for which the value of $|\sin\delta|$ is being measured. The direction S makes an angle ϑ with the optic axis OA.

Considering the relations defining the two possible phase velocities v'_p and v''_p for a given propagation direction S (see Appendix *A*, which includes a list of symbol definitions),

$$v'^2_p = v^2_o \tag{9}$$

and

$$v''^2_p = v^2_o \cos^2\vartheta + v^2_e \sin^2\vartheta, \tag{10}$$

we can derive the following expression:

$$v_{\rm p}'^2 - v_{\rm p}''^2 = \left(v_{\rm o}^2 - v_{\rm e}^2\right)\sin^2\vartheta. \tag{11}$$

Using refractive indices instead of velocities, we obtain

$$\frac{1}{n'^2} - \frac{1}{n''^2} = \left(\frac{1}{n_{\rm o}^2} - \frac{1}{n_{\rm e}^2}\right)\sin^2\vartheta. \tag{12}$$

Since the value of the birefringence $\Delta n = n_{\rm e} - n_{\rm o}$ is generally a small quantity, we may write with reasonable accuracy the value of the birefringence Δn_S (in general the plano-birefringence) measured down the direction of propagation S as

$$\Delta n_S \simeq (n_{\rm e} - n_{\rm o})\sin^2\vartheta. \tag{13}$$

Using spherical trigonometry with the right triangle OA–S–A illustrated in Fig. 3, we can write the following equation:

$$\cos\vartheta = \cos\psi_1\cos\psi_2. \tag{14}$$

In Fig. 3, ψ_1 is the component angle of S measured from the z axis projected on the principal section PS (OA–A). ψ_2 is the component angle of S measured from the z axis projected on the plane perpendicular to PS (OA–B), which is also equal to S–A. Thus equation (13) becomes

$$\Delta n_S \simeq \Delta n\left(1 - \cos^2\psi_1\cos^2\psi_2\right). \tag{15}$$

Using the Metripol technique, we actually measure $|\sin\delta|$ and therefore we can write

$$\left|\sin\delta_S\right| \simeq \left|\sin\left(\frac{2\pi}{\lambda}\Delta n_S t\right)\right|, \tag{16}$$

where $\left|\sin\delta_S\right|$ denotes the value of $|\sin\delta|$ measured down the direction of propagation S within the sample. Thus equation (15) becomes

$$\left|\sin\delta_S\right| \simeq \left|\sin\left[\frac{2\pi t}{\lambda}\Delta n\left(1 - \cos^2\psi_1\cos^2\psi_2\right)\right]\right|. \tag{17}$$

Fig. 4 is a stereographic representation of the optical indicatrix for a uniaxial sample for two different positions of the microscope tilting-stage, S' and S. The directions S' and S make angles ϑ' and ϑ with the optic axis OA, respectively. Assuming that the position S' denotes the direction of propagation of the light normal to the sample, *i.e.* before tilting, and position S represents the direction of propagation after tilting, we can decompose angles ψ_1 and ψ_2 into two components in the following way:

$$\psi_1 = \theta_1 + \omega_1 \tag{18}$$

$$\psi_2 = \theta_2 + \omega_2. \tag{19}$$

Thus equation (17) may be written in the following form:

$$|\sin\delta_S| \simeq \left|\sin\left\{\frac{2\pi t}{\lambda}\Delta n\left[1 - \cos^2(\theta_1 + \omega_1)\cos^2(\theta_2 + \omega_2)\right]\right\}\right|. \tag{20}$$

In equation (20) angles ω_1 and ω_2 are internal tilt angles measured along the principal section PS and the plane perpendicular to PS, respectively. Angles θ_1 and θ_2 are the component angles of S' measured from the z axis projected on the principal section PS and the plane perpendicular to PS, respectively.

Note that the two internal tilt angles ω_1 and ω_2 are different from the corresponding external tilt angles Ω_1 and Ω_2, which are defined by the tilting of the stage and, in general, do not coincide with Θ_1 and Θ_2. In contrast to the external tilt angles, for any specified propagation direction S, the internal tilt angles depend on the refractive indices of the sample. Thus internal tilt angles are those measured within the sample where the light is refracted.

To obtain the values of internal tilt angles, we can assume a mean refractive index $n_{\rm mean}$ of the sample and use Snell's law. The equations that we use to convert external tilt angles to internal tilt angles are written in the following form:

$$\omega_1 \simeq \sin^{-1}\left(\frac{\sin\Omega_1}{n_{\rm mean}}\right), \quad \omega_2 \simeq \sin^{-1}\left(\frac{\sin\Omega_2}{n_{\rm mean}}\right). \tag{21}$$

In uniaxial crystals, the mean refractive index of the sample may be calculated as (Wahlstrom, 1965)

$$n_{\rm mean} = \frac{(2n_{\rm o} + n_{\rm e})}{3}. \tag{22}$$

For crystals with a large difference between the maximum and minimum refractive indices, the mean refractive index of the uniaxial sample takes the following form:

$$n_{\rm mean} = (n_{\rm o}^2 n_{\rm e})^{1/3}. \tag{23}$$

Taking into account equations (21), equation (20) becomes

$$|\sin\delta_S| \simeq \left|\sin\left[\frac{2\pi t}{\lambda}\Delta n\left(1 - \left\{\cos^2\left[\theta_1 + \sin^{-1}\left(\frac{\sin\Omega_1}{n_{\rm mean}}\right)\right]\times\cos^2\left[\theta_2 + \sin^{-1}\left(\frac{\sin\Omega_2}{n_{\rm mean}}\right)\right]\right\}\right)\right]\right| \tag{24}$$

From Fig. 4, we see that by redefining the x and y axes so that y' lies along PS′, the component angle θ_2' for the inclination angle ϑ' is then equal to zero and the corresponding component angle θ_1' becomes equivalent to ϑ'. Note that in this case

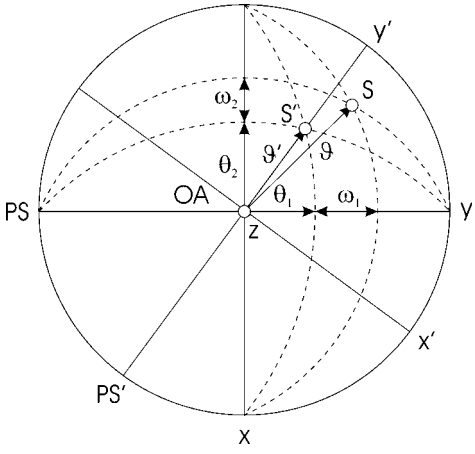

Figure 4
Stereographic representation of the optical indicatrix for a uniaxial sample for two different positions of the microscope tilting-stage, S' and S. PS′ denotes the principal section which contains the optic axis OA and the direction of propagation S'.

θ_1' is equal to the angle of the sample normal with respect to the optic axis OA. Assuming additionally that the tilting is performed only along the principal section PS′, equation (24) may be written in a less complicated form to simplify the analysis:

$$|\sin\delta_S| \simeq \left|\sin\left\{\frac{2\pi t}{\lambda}\Delta n\,\sin^2\left[\vartheta' + \sin^{-1}\left(\frac{\sin\Omega_1'}{n_{\rm mean}}\right)\right]\right\}\right|, \quad (25)$$

where Ω_1' is the external tilt angle measured along the principal section PS′.

Note that if the external tilt angles are small, equation (24) becomes

$$|\sin\delta_S| \simeq \left|\sin\left(\frac{2\pi t}{\lambda}\Delta n\left\{1-\left[\cos^2\left(\theta_1+\frac{\Omega_1}{n_{\rm mean}}\right)\times\cos^2\left(\theta_2+\frac{\Omega_2}{n_{\rm mean}}\right)\right]\right\}\right)\right| \quad (26)$$

and equation (25) takes the following form:

$$|\sin\delta_S| \simeq \left|\sin\left[\frac{2\pi t}{\lambda}\Delta n\,\sin^2\left(\vartheta'+\frac{\Omega_1'}{n_{\rm mean}}\right)\right]\right|. \quad (27)$$

Taking into account the ambiguity expressed by equations (4) and (5), we can write equation (25) in the following form:

$$|\delta_S| = \delta_{0S} + m\pi \simeq \left|\frac{2\pi t}{\lambda}\Delta n\,\sin^2\left[\vartheta' + \sin^{-1}\left(\frac{\sin\Omega_1'}{n_{\rm mean}}\right)\right]\right| \quad (28a)$$

and

$$|\delta_S| = -\delta_{0S} + m\pi \simeq \left|\frac{2\pi t}{\lambda}\Delta n\,\sin^2\left[\vartheta' + \sin^{-1}\left(\frac{\sin\Omega_1'}{n_{\rm mean}}\right)\right]\right| \quad (28b)$$

for positive and negative slopes of the $|\sin\delta|$ function, respectively. In equations (28), δ_{0S} denotes the relative phase difference measured down the direction of propagation S within the sample.

It is worth pointing out here that in a conventional universal stage, it is usual to place glass hemispheres above and below the sample in order to try to compensate for the effect of the average refractive index of the sample; however, this also means that the match is poor for samples with refractive indices different from that of glass, and so this is a serious limitation to the use of a conventional universal stage. The inclusion of $n_{\rm mean}$ in our equations effectively acts in the same way; although here, because it is a freely variable quantity, we have complete flexibility in its value.

Note also that if the thickness of the sample t or the tilt angles are significant, then a thickness correction should be applied to the equations derived above. However, usually this correction is very small and can be neglected. If it is required then consider Fig. 5. This illustrates a sample slice tilted through the external tilt angle Ω_1'. ω_1' is the corresponding internal tilt angle measured within the sample. $t_{\rm eff}$ denotes the path length traveled by light within the sample. Using trigonometry with Fig. 5, the equation for the effective thickness becomes

$$t_{\rm eff} = \frac{t}{\cos(\omega_1' - \Omega_1')}. \quad (29)$$

2.2. Sign of the optical indicatrix

Using the Metripol technique, we actually measure $|\sin\delta|$ and therefore we have to consider the ambiguity expressed by equations (4) and (5). The azimuthal angle ϕ is defined as the orientation angle of one of the axes of a section of the optical indicatrix measured from a predetermined direction, and each time $|\sin\delta|$ passes through zero, the computed value ϕ changes through 90°. Moreover, when $|\sin\delta|$ passes through 1, the value of m increases or decreases (Geday & Glazer, 2002). Fig. 6 illustrates the dependence between the value of m and the azimuthal angle ϕ for quartz. The simulation was carried out using the following equation:

$$|\sin\delta_S| \simeq \left|\sin\left[\frac{2\pi t}{\lambda}\Delta n\,\sin^2(\theta_1'+\omega_1')\right]\right|, \quad (30)$$

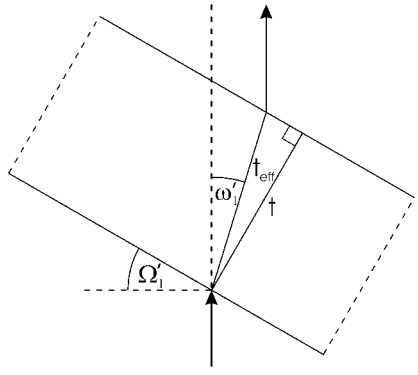

Figure 5
Light path within a sample slice tilted through the angle Ω_1'.

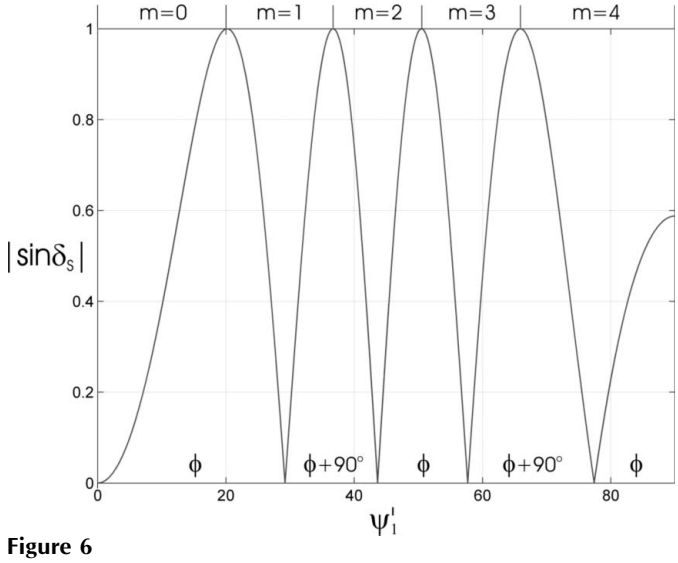

Figure 6
Simulation of the dependence between the value of m and the azimuthal angle ϕ for quartz with thickness equal to 0.14 mm.

which is recast from equation (25) and represents the $|\sin\delta|$ function in the principal section PS′. In the simulation we assumed literature values for the refractive indices and a wavelength equal to 600 nm. Furthermore, the thickness of the sample was taken as a fixed value equal to 0.14 mm.

In the figure, $|\sin\delta|$ is presented as a function of the component angle $\psi_1' = \theta_1' + \omega_1'$, changing from 0 to 90°. For $m = 0$, for which the ambiguity does not appear in both the relative phase difference δ_{0S} and the azimuthal angle ϕ, we normally set up the Metripol microscope so that ϕ measures the orientation of the slow axis of the relevant section of the optical indicatrix.

The sign of the optical indicatrix may then be determined by considering the value of the azimuthal angle ϕ for a specified slope of the $|\sin\delta|$ function and m, as well as properties of the uniaxial optical indicatrix. If the sign of the optical indicatrix is positive, the extraordinary refractive index n_e is greater than n_o. The radial component n_e' of a section of the optical indicatrix when the direction of propagation is along the optic axis OA is equal to n_o and increases when the inclination angle with respect to the optic axis increases. For a direction of propagation perpendicular to the optic axis, $n_e' = n_e$. This also means that in the case of a positive sign, the radial component n_e' is the slow axis (greater refractive index) of a section of the optical indicatrix. In the case of a negative sign where the extraordinary refractive index $n_e < n_o$, the situation is opposite and the radial component n_e' is the fast axis (smaller refractive index) of a section of the optical indicatrix.

Table 1 shows the dependence between m and the azimuthal angle ϕ for both optically positive and optically negative uniaxial crystals.

Thus, by considering the value of the azimuthal angle ϕ for a specified slope of the $|\sin\delta|$ function and a specified value of m, we can easily determine the sign of the optical indicatrix (see §2.4).

2.3. Data analysis

As shown below, the tilting-stage technique allows us to obtain precise three-dimensional birefringence information for uniaxial samples. Using this method, we are able to extract a precise value for the inclination angle ϑ' of the optic axis OA. It is also possible to estimate the mean refractive index n_{mean}. Moreover, the actual values of the phase difference δ_S, and thus optical retardance $\Delta n_S t$ and birefringence Δn_S, may be determined from the measured $|\sin\delta_S|$ values without the necessity of using multiwavelength methods.

The algorithm presented below explains the sequence of steps.

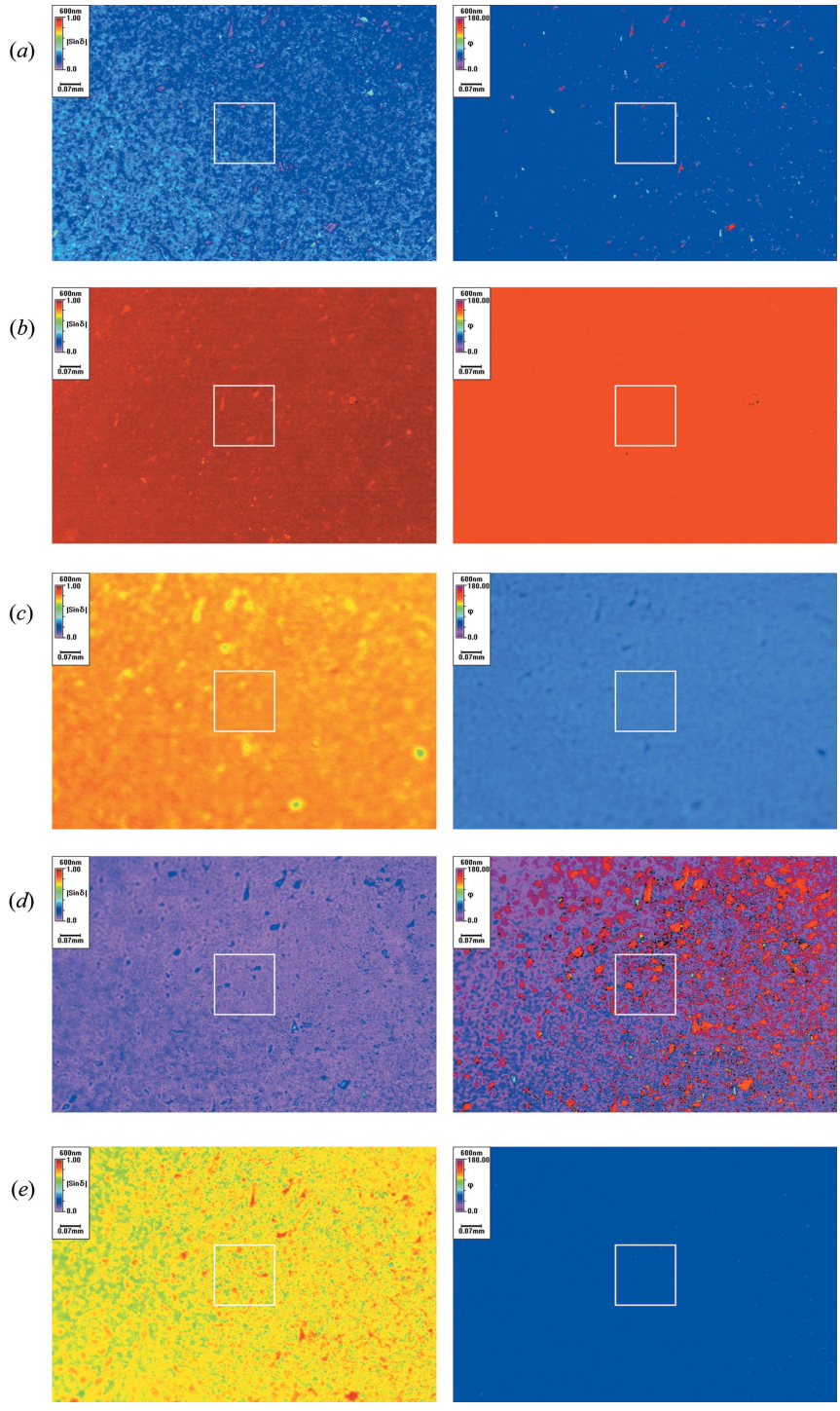

Figure 7
$|\sin\delta|$ and azimuthal angle ϕ images collected on a sample of quartz with approximate orientation 45° to the [0001] direction and thickness 0.14 mm, for different tilt angles Θ_1 and Θ_2 of the tilting-stage: (*a*) $\Theta_1 = 0°$ and $\Theta_2 = 0°$, (*b*) $\Theta_1 = -10°$ and $\Theta_2 = -10°$, (*c*) $\Theta_1 = -10°$ and $\Theta_2 = 10°$, (*d*) $\Theta_1 = 10°$ and $\Theta_2 = -10°$, (*e*) $\Theta_1 = 10°$ and $\Theta_2 = 10°$.

Step 1. Collect data on the Metripol for many tilt angles of the uniaxial sample within a specified range of the two perpendicular tilt axes Θ_1 and Θ_2 of the tilting-stage. Fig. 7 presents a few $|\sin\delta|$ and ϕ images for a quartz sample for different tilt angles Θ_1 and Θ_2. Note that these images were chosen from a large number of collected images. The rectangles shown in the figures represent the sets of pixels for which average values of $|\sin\delta|$ and the azimuthal angle ϕ were calculated.

Step 2. Note that for any general alignment of the sample, the two tilt axes Θ_1 and Θ_2 of the tilting-stage will not necessarily be parallel or perpendicular to any principal section PS. In this case, to perform the analysis it is necessary to make an azimuthal transformation of the tilt axes Θ_1 and Θ_2 *via* transformation with a rotation matrix. Since the

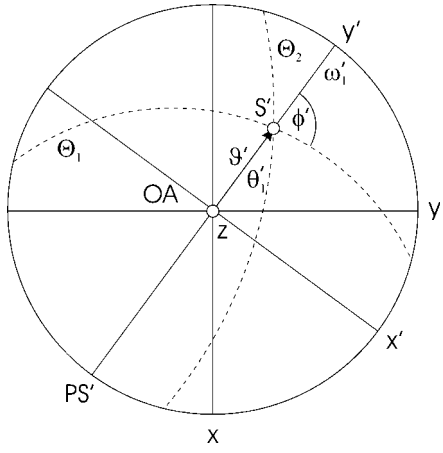

Figure 8
Stereographic representation of the optical indicatrix for a uniaxial sample with the principal section PS′ and two perpendicular tilt axes Θ_1 and Θ_2 of the microscope tilting-stage (the traces of the tilt axes are shown here as great circles). The azimuthal angle ϕ' corresponds to the propagation direction S'.

Table 1
Dependence between m and the azimuthal angle ϕ for optically positive and negative uniaxial crystals.

		Positive indicatrix		Negative indicatrix	
Slope	m value	ϕ value	ϕ direction	ϕ value	ϕ direction
Positive	0	ϕ	Radial	ϕ	Tangential
Negative	1	ϕ	Radial	ϕ	Tangential
Positive	1	$\phi \pm 90^\circ$	Tangential	$\phi \pm 90^\circ$	Radial
Negative	2	$\phi \pm 90^\circ$	Tangential	$\phi \pm 90^\circ$	Radial
Positive	2	ϕ	Radial	ϕ	Tangential
Negative	3	ϕ	Radial	ϕ	Tangential
Positive	3	$\phi \pm 90^\circ$	Tangential	$\phi \pm 90^\circ$	Radial
Negative	4	$\phi \pm 90^\circ$	Tangential	$\phi \pm 90^\circ$	Radial
...	...	...	...	...	...

Metripol gives a value of the azimuthal angle ϕ of one of the axes of a section of the optical indicatrix for each position of the tilting-stage, it is always possible to find these directions. As mentioned above, in order to simplify the process of analysis it is convenient to find a new principal section PS′ for which θ'_2 is equal to zero, *i.e.* the new principal section PS′ contains the optic axis OA and the direction of propagation S'. Then the component angle θ'_1 becomes equal to the angle of the sample normal with respect to the optic axis OA. In order to accomplish this it is necessary first to find the value of the azimuthal angle ϕ' corresponding to the propagation direction S' (Fig. 8) and subsequently to rotate the tilt axes Θ_1 and Θ_2 through the angle ϕ', thus:

$$\begin{pmatrix} \Omega'_1 \\ \Omega'_2 \end{pmatrix} = \begin{pmatrix} \cos\phi' & \sin\phi' \\ -\sin\phi' & \cos\phi' \end{pmatrix} \begin{pmatrix} \Theta_1 \\ \Theta_2 \end{pmatrix}. \tag{31}$$

Note that, as mentioned earlier, the value of the azimuthal angle changes through 90° when $|\sin\delta|$ passes through zero. Therefore, the ambiguity introduced *via*

$$\phi' \pm 90^\circ \tag{32}$$

should also be taken into account.

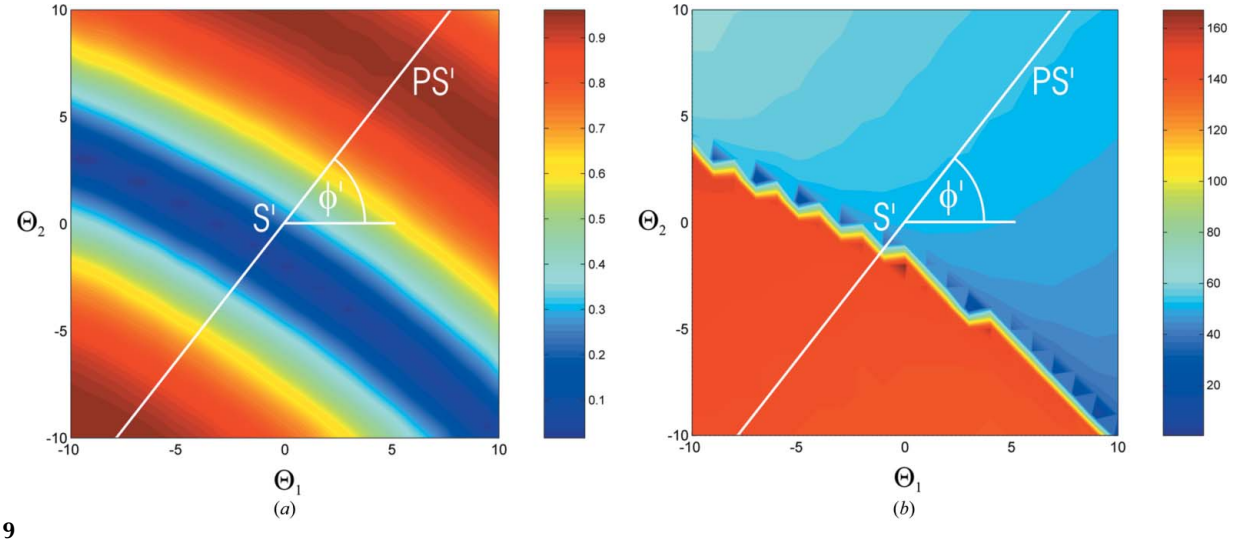

Figure 9
(*a*) $|\sin\delta|$ and (*b*) ϕ as a function of the two external tilt angles Θ_1 and Θ_2 for a quartz plate with approximate orientation 45° to the [0001] direction and thickness 0.14 mm. The measurement was carried out at a wavelength of 600 nm and a total of 441 tilt angles were used. The complete set of measurements with the current set-up took 55 min. The azimuthal angle ϕ' determining the position of the principal section PS′ is found to be equal to 51.1°. PS′ is denoted here by a thick white line.

Step 3. Interpolate the measured $|\sin\delta|$ values along the principal section PS′.

Step 4. Apply non-linear curve fitting to the data in the principal section PS′ using equations (28) in order to obtain the value of the birefringence $\Delta n = n_e - n_o$, the inclination angle ϑ' with respect to the optic axis OA, and the mean refractive index n_{mean} of the uniaxial sample. Using the Metripol technique, we actually measure $|\sin\delta|$ and therefore we have to take into account the fact that m in equation (5) is not known. However, by knowing that the inclination angle ϑ' ranges from 0 to 90° and the mean refractive index n_{mean} typically varies from 1.5 to 2.2, we choose only the physically reasonable solutions for different positive values of m.

2.4. Three-dimensional birefringence information

Fig. 9 presents results for a quartz section, roughly 45° to the [0001] direction and with thickness 0.14 mm, which were obtained using the tilting-stage technique. The figure shows a graphical representation of $|\sin\delta|$ and ϕ as a function of Θ_1 and Θ_2. The measurement was carried out at a wavelength of 600 nm. It is important to understand that the data used for this plot were taken only from a small portion of the actual images collected for the quartz sample (see rectangle marked in Fig. 7).

In order to analyze the data further, we applied non-linear curve fitting to the data in the principal section PS′ using equations (28) to obtain the values of the birefringence Δn, the inclination angle ϑ' and the mean refractive index n_{mean} for different positive values of m. The estimated values of the birefringence Δn, the inclination angle ϑ' and the mean refractive index n_{mean} are sensitive to an error in determining the position of the principal section PS′. However, usually we can obtain very precise values of the azimuthal angle and this error can be neglected. We also observe that the estimated value of the birefringence Δn very strongly depends on the accuracy with which the thickness of the sample is being measured. Usually this error has a very small influence on the estimated values of the inclination angle ϑ' and the mean refractive index n_{mean}. Moreover, if the thickness of the sample or the tilt angles are significant, then a thickness correction expressed by equation (29) should be applied. However, usually this correction is extremely small and very often can be neglected. The most significant error appears when the values of Δn, ϑ' and n_{mean} are refined simultaneously using equations (28). All the parameters, and especially ϑ' and n_{mean}, are correlated. The correlation between these two parameters and Δn increases rapidly when $\vartheta' \rightarrow 0°$. Fixing the value of n_{mean} improves the curve fitting radically, and Δn and ϑ' are then refined to high precision.

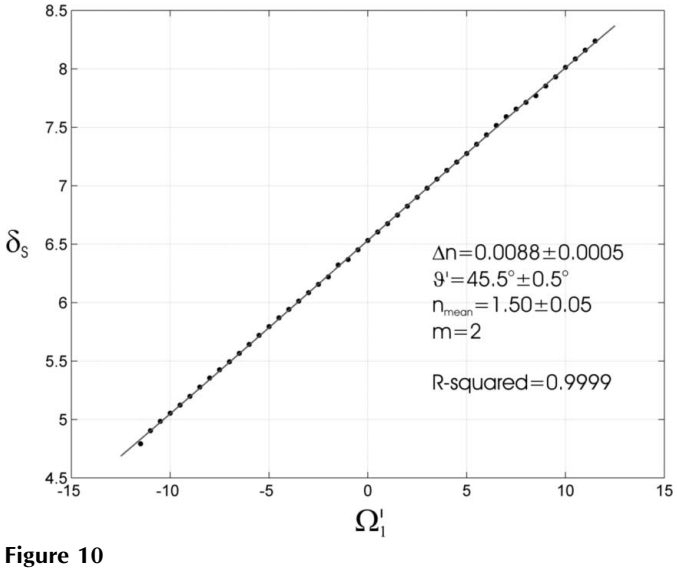

Figure 10
Non-linear curve fitting applied to the data in the principal section PS′ using equations (28) for $m = 2$.

Table 2
Estimated values of the birefringence Δn, the inclination angle ϑ', and the mean refractive index n_{mean} for different positive values of m.

m	Birefringence, Δn	Inclination angle, ϑ' (°)	Refractive index, n_{mean}	R-squared
0	800370	0	8386	0.8816
1	0.0046	44.9	0.78	0.9998
2	**0.0088**	**45.5**	**1.50**	**0.9999**
3	0.0128	45.8	2.20	0.9999
4	0.0168	46.1	2.90	0.9999
5	0.0208	46.4	3.57	0.9999
6	0.0246	46.7	4.24	0.9999
7	0.0284	46.9	4.89	0.9999
8	0.0322	47.2	5.54	0.9999

Fig. 10 shows an example of non-linear curve fitting applied to the data in the principal section PS′ for $m = 2$.

Table 2 gives the values of the estimated parameters for different positive values of m. By analyzing the results, we choose only physically reasonable solutions corresponding to the most probable values of Δn, ϑ' and n_{mean}.

In Table 2 there is only one physically likely solution, *i.e.* $m = 2$. In order to determine the sign of the optical indicatrix, we consider the value of the azimuthal angle $\phi' = 51.1°$ for a specified slope of the $|\sin\delta|$ function and $m = 2$, as well as properties of the optical indicatrix. From Fig. 9 we see that the contours form approximately concentric circles around the optic axis (situated off the diagram in the bottom left direction). The point S' corresponding to $\Theta_1 = \Theta_2 = 0°$ is seen to lie on the positive slope of the $|\sin\delta|$ measured in the direction away from the optic axis (towards the upper right). By considering Fig. 6 and Table 1, we can unambiguously assign the optical indicatrix of the sample as positive with the birefringence $\Delta n = +0.0088$. This also means that the actual values of the phase difference δ_S, and thus optical retardance $\Delta n_S t$ and birefringence Δn_S, are positive.

This method gives a value for the birefringence Δn that corresponds well with the literature value of 0.009 (see for example, Deer *et al.*, 1992). Furthermore, the inclination angle ϑ' with respect to the optic axis OA is estimated well, almost independently of m.

Note that for a single crystal it is sufficient to measure $|\sin\delta|$ only along the principal section PS′. This is in principle easily found from the values ϕ' and $\phi' \pm 90°$. However, by collecting

data for the whole range of tilt angles, the observed curvature of the $|\sin\delta|$ contours makes it possible to locate the optic axis OA. In addition, when the sample is unknown, this allows us to distinguish between uniaxial and biaxial samples.

2.5. Preferred orientation of polycrystalline materials

Most polycrystalline materials show preferred orientation (also called texture) of their crystallites. The crystallites are often referred to as grains. The preferred orientation is an important feature and has a decisive influence on the anisotropy of physical properties such as light refraction, piezoelectricity, electrical conductivity, magnetic susceptibility, *etc.* (Wenk & Van Houtte, 2004). Several methods already exist for measuring preferred orientation, but they all currently have disadvantages: (i) X-ray or neutron pole-figure measurements of large samples provide an excellent measure of the statistical preferred orientation, but normally provide no spatial resolution;[3] (ii) electron backscatter diffraction (EBSD) using a scanning electron microscope provides both full crystallographic orientation and spatial resolution on a pixel basis, but only for small areas and only after very time-consuming preparation (chemical–mechanical polishing). Mancktelow (1987) has shown that samples of quartzite taken from alpine regions of Switzerland exhibit preferred orientation in grains of quartz that can be measured by using optical orientation information obtained with representative microscope sections and a conventional universal stage. The results reproduce well equivalent measurements made with X-ray pole-figure studies on large pieces of rock. Mancktelow revealed an interesting correlation with different regions of the Alps in connection with theories on the early history of mountain development.

One of the most important advantages of our tilting-stage technique is that it enables us to obtain precise information on the preferred orientation as well as on the birefringence of the crystallites; it can easily detect any changes in anisotropy caused by strain and deformations formed during growth of the polycrystalline material. Moreover, any changes occurring as a result of recrystallization or phase transformations can be precisely recorded and analyzed.

In order to demonstrate this, we carried out Metripol measurements on one of the quartzite samples (SP217) used by Mancktelow. Our experiments have successfully produced results consistent with his own. Moreover, our results provide much more information on the anisotropy of the polycrystalline sample.

With the Metripol technique, each grain of the polycrystalline specimen can be analyzed to very high precision. The highest possible resolution which can be achieved by the current optical system is equal to 0.3 μm with a 50× objective. Note also that the tilting-stage technique enables us to obtain precise values of both plano-birefringence, $n'' - n'$, and birefringence, $n_e - n_o$, for each grain of the sample, and any changes caused by *e.g.* strain or deformation can be precisely detected and analyzed.

[3] However, some X-ray techniques such as topography do provide spatially resolved images.

Fig. 11 illustrates three types of images measured for a part of the quartzite sample with thickness 0.019 mm. The images correspond to the external tilt angles Θ_1 and Θ_2 of the tilting-stage set equal to zero. The first image gives quantitative information on $|\sin\delta|$, the second image shows the azimuthal angle ϕ of one of the axes of a section of the optical indicatrix measured from a predetermined direction (horizontal direc-

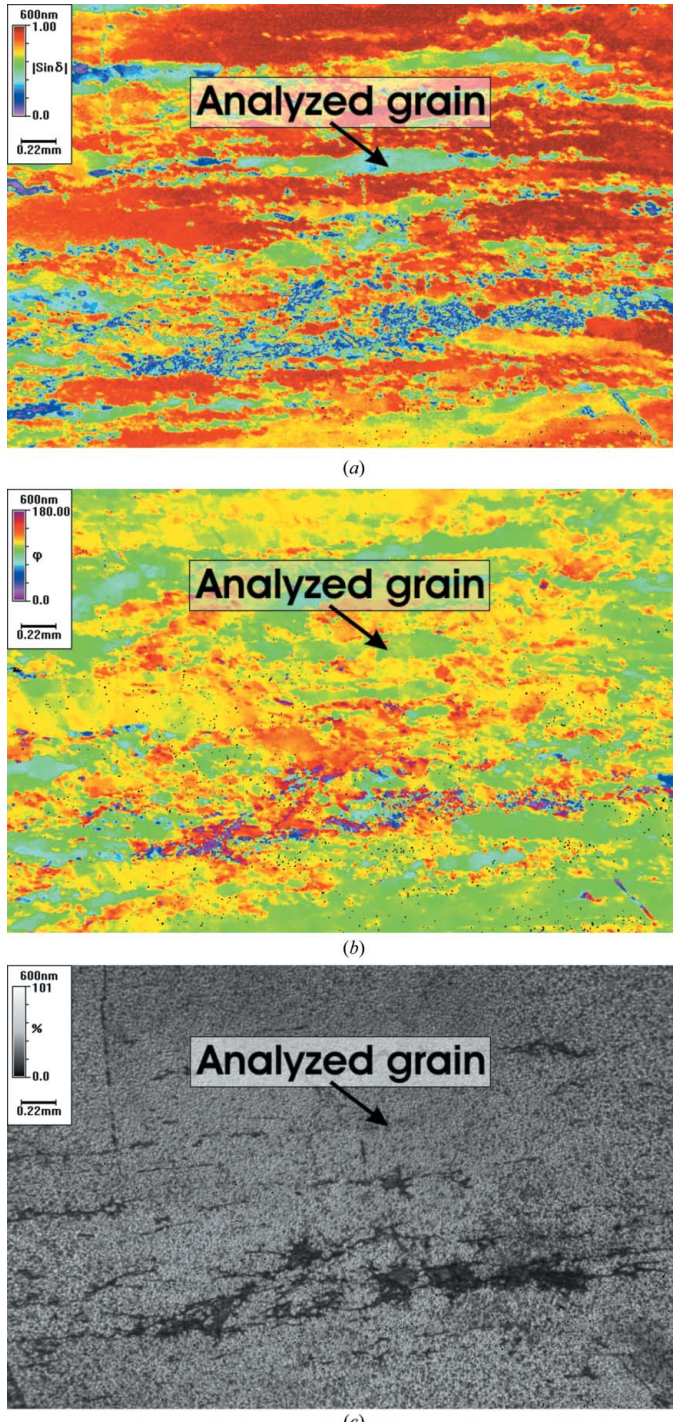

Figure 11
Sample images of (*a*) $|\sin\delta|$, (*b*) azimuthal angle ϕ and (*c*) light transmission I_0 for a region of the alpine quartzite sample SP217 with thickness 0.019 mm. The images correspond to the external tilt angles Θ_1 and Θ_2 of the tilting-stage set equal to zero.

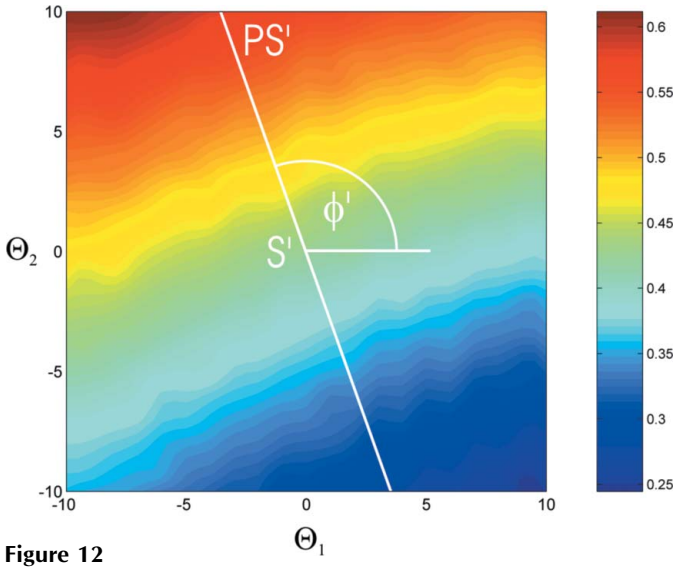

Figure 12
$|\sin\delta|$ as a function of the two external tilt angles Θ_1 and Θ_2 of the tilting-stage for one single grain (marked in Fig. 11) of the quartzite sample SP217.

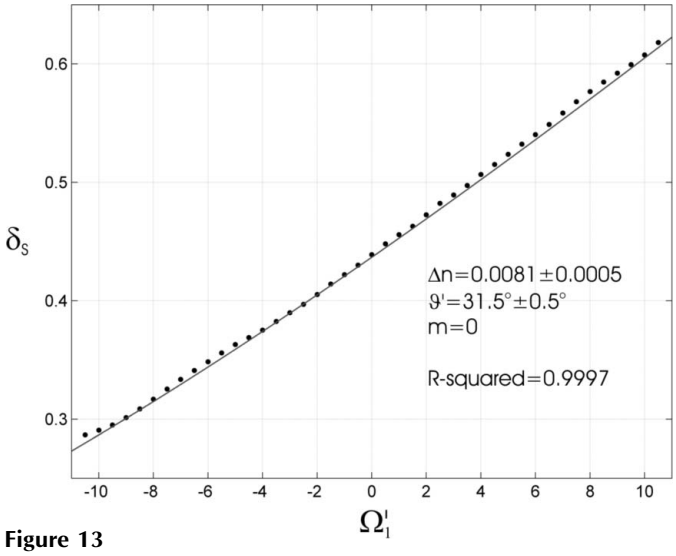

Figure 13
Non-linear curve fitting applied to the data in the principal section PS′ obtained from the single grain (marked in Fig. 11) of the quartzite sample.

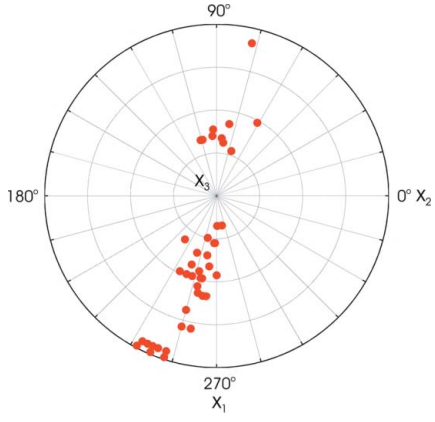

Figure 14
Stereographic plot showing texture in the quartzite sample SP217 (42 data points).

tion within the image), and the last one shows the light transmission I_0 through the specimen.

Fig. 12 shows a graphical representation of $|\sin\delta|$ as a function of Θ_1 and Θ_2 for one single grain of the quartzite sample (marked in Fig. 11). The azimuthal angle ϕ' determining the position of the principal section PS′ for this particular grain is equal to 109°. The measurement was carried out at a wavelength of 600 nm and a total of 441 tilt angles were used. The optic axis in this case is situated towards the bottom right direction as judged by the curvature of the contours.

Fig. 13 shows the non-linear curve fitting applied to the data for this particular grain along the principal section PS′ using equations (28) to obtain the value of Δn and ϑ' with respect to the optic axis OA. In order to obtain precise values of ϑ' for all grains in the image, the mean refractive index $n_{\rm mean}$ of the quartzite sample was taken as a fixed value, equal to 1.547, using literature values of the ordinary refractive index $n_{\rm o}$ and the extraordinary refractive index $n_{\rm e}$. Fixing the mean refractive index in this way improves the location of the correct minimum in the curve-fitting process and allows reliable comparison of orientation information between all the grains studied. By applying non-linear curve fitting to the data using equations (28) for different positive values of m, we found only one physically reasonable solution for each grain, corresponding to the most probable value of the birefringence Δn and the inclination angle ϑ'.

Fig. 14 is a stereographic plot of the angles ϑ' for many different grains, showing the preferred orientation characteristic of grains in this particular quartzite sample. In the figure, the x_3 axis is perpendicular to the foliation of the sample, while the x_1 axis lies within the foliation and is perpendicular to the lineation of the sample. The x_2 axis also lies within the foliation and is parallel to the lineation of the sample.

3. Conclusions

We have shown that by combining a computer-controlled two-axis tilting-stage on a microscope with the Metripol technique, it is possible to collect reliable three-dimensional data for $|\sin\delta|$ and azimuthal angle ϕ in order to obtain precise three-dimensional birefringence information for optically uniaxial samples in any general alignment.

The following information can be obtained from the above technique.

(i) Two-dimensional projections of lines of equal birefringence.

(ii) A precise value of the birefringence $\Delta n = n_{\rm e} - n_{\rm o}$.

(iii) A precise value for the orientation of the optic axis ϑ'.

(iv) The actual values of the phase difference δ_S, and thus optical retardance $\Delta n_S t$ and birefringence Δn_S.

(v) An estimate of the mean refractive index of the sample $n_{\rm mean}$, and hence all the refractive indices.

(vi) The sign of the optical indicatrix.

(vii) Whether the sample is uniaxial or biaxial.

(viii) Texture information from a polycrystalline material.

(ix) Identification, or at least classification within a specific group of crystalline materials, of unknown samples.

This method has also been applied to the more complicated case of optically biaxial materials; this will be the subject of a later publication.

APPENDIX *A*

A1. Relations defining the phase velocities

Maxwell's equations for a nonmagnetic, homogeneous and transparent medium are defined by the following relations between the electric field **E**, the electric displacement **D**, the magnetic field **H** and the magnetic induction **B**:

$$-\mu_0 \frac{\partial \mathbf{H}}{\partial t} = \nabla \times \mathbf{E},$$

$$\frac{\partial \mathbf{D}}{\partial t} = \nabla \times \mathbf{H},$$

$$\nabla \cdot \mathbf{D} = 0,$$

$$\nabla \cdot \mathbf{H} = 0. \tag{33}$$

For plane monochromatic waves given by

$$\mathbf{E} = \mathbf{E}_0 \exp[i(\mathbf{k} \cdot \mathbf{r} - \omega t)], \tag{34}$$

we obtain from Maxwell's equations:

$$\mu_0 i\omega \mathbf{H} = i(\mathbf{k} \times \mathbf{E}),$$

$$-i\omega \mathbf{D} = i(\mathbf{k} \times \mathbf{H}). \tag{35}$$

In addition: (i) vector **D** is perpendicular to the direction of the wavevector **k** determining the propagation of the surface of constant phase; (ii) vectors **D**, **E**, **k** and the Poynting vector $\mathbf{S} = \mathbf{E} \times \mathbf{H}$ are coplanar; (iii) vectors **S** and **k** do not normally coincide in direction.

From equations (35) and

$$k^2 = \frac{\omega^2}{c^2} n^2, \quad \mathbf{k} = k\mathbf{s}, \quad |\mathbf{s}| = 1, \tag{36}$$

we obtain

$$\varepsilon_i E_i = n^2[E_i - s_i(\mathbf{s} \cdot \mathbf{E})], \quad \text{where } i = 1, 2, 3. \tag{37}$$

This then leads to the result

$$\frac{s_1^2}{n^2 - \varepsilon_1} + \frac{s_2^2}{n^2 - \varepsilon_2} + \frac{s_3^2}{n^2 - \varepsilon_3} = \frac{1}{n^2}. \tag{38}$$

From equation (38) and

$$s_1^2 + s_2^2 + s_3^2 = 1, \quad v_i = \frac{c}{(\varepsilon_i)^{1/2}}, \quad v_\mathrm{p} = \frac{c}{n}, \tag{39}$$

the Fresnel equation for the velocity of phase propagation of electromagnetic waves in an anisotropic medium (Born & Wolf, 1999) is obtained:

$$\frac{s_1^2}{v_\mathrm{p}^2 - v_1^2} + \frac{s_2^2}{v_\mathrm{p}^2 - v_2^2} + \frac{s_3^2}{v_\mathrm{p}^2 - v_3^2} = 0. \tag{40}$$

For uniaxial crystals,

$$v_\mathrm{o} = \frac{c}{n_\mathrm{o}} = \frac{c}{[\varepsilon^{(\mathrm{o})}]^{1/2}},$$

$$v_\mathrm{e} = \frac{c}{n_\mathrm{e}} = \frac{c}{[\varepsilon^{(\mathrm{e})}]^{1/2}}, \tag{41}$$

and so

$$\left(s_1^2 + s_2^2\right)\left(v_\mathrm{p}^2 - v_\mathrm{o}^2\right)\left(v_\mathrm{p}^2 - v_\mathrm{e}^2\right) + s_3^2\left(v_\mathrm{p}^2 - v_\mathrm{o}^2\right)^2 = 0. \tag{42}$$

Let ϑ denote the angle between the vector **S** and the optic axis. Then

$$s_1^2 + s_2^2 = \sin^2 \vartheta,$$

$$s_3^2 = \cos^2 \vartheta, \tag{43}$$

and then the following equation is obtained:

$$\left(v_\mathrm{p}^2 - v_\mathrm{o}^2\right)\left(v_\mathrm{p}^2 - v_\mathrm{e}^2\right) \sin^2 \vartheta + \left(v_\mathrm{p}^2 - v_\mathrm{o}^2\right) \cos^2 \vartheta = 0. \tag{44}$$

The two roots of this equation are given by (Petykiewicz, 1992)

$$v_\mathrm{p}'^2 = v_\mathrm{o}^2,$$

$$v_\mathrm{p}''^2 = v_\mathrm{o}^2 \cos^2 \vartheta + v_\mathrm{e}^2 \sin^2 \vartheta. \tag{45}$$

In uniaxial crystals there are two wave velocity surfaces. The first is a sphere and corresponds to the ordinary wave, with the propagation velocity independent of the direction of propagation. The second is an ellipsoid and corresponds to the extraordinary wave with the propagation velocity depending on the angle between the direction of the wavevector **k** and the optic axis.

A2. List of symbols

δ: phase difference.

λ: wavelength of the light.

$n'' - n'$: effective birefringence projected onto the plane of the sample; the so-called plano-birefringence.

t: thickness of the sample.

I: intensity of the light measured at any position within the image captured by the CCD camera.

I_0: intensity of unpolarized light transmitted through the sample.

ϕ: orientation angle of one of the axes of a section of the optical indicatrix measured from a predetermined direction; the so-called azimuthal angle.

α: angular orientation of the rotating polarizer.

δ_0: relative phase difference.

m: positive integer.

$\delta_{0,1}$, $\delta_{0,2}$: values of the relative phase difference measured at two different wavelengths λ_1 and λ_2, respectively.

δ_1: absolute value of the phase difference calculated for the wavelength λ_1.

Θ_1, Θ_2: two perpendicular external tilt angles of the tilting-stage.

OA: optic axis.

n_o: ordinary refractive index.

n_e: extraordinary refractive index.

S: general direction of propagation of the light within the sample.

PS: principal section containing the optic axis OA.

ϑ: angle between the direction of propagation S and the optic axis OA.

v'_p, v''_p: two possible phase velocities for a given propagation direction S.

v_o: phase velocity corresponding to the ordinary refractive index.

v_e: phase velocity corresponding to the extraordinary refractive index.

n', n'': two possible refractive indices for a given propagation direction S.

$\Delta n = n_e - n_o$: birefringence.

Δn_S: plano-birefringence measured down the direction of propagation S.

δ_S: phase difference corresponding to the direction of propagation S.

$|\sin\delta_S|$: $|\sin\delta|$ measured down the direction of propagation S.

ψ_1: component angle of S measured from the z axis projected on the principal section PS.

ψ_2: component angle of S measured from the z axis projected on the plane perpendicular to the principal section PS.

S': direction of propagation of the light normal to the sample, *i.e.* before tilting.

ϑ': angle between the direction of propagation S' and the optic axis OA, equal to the angle of the sample normal with respect to the optic axis OA.

θ_1: component angle of S', measured from the z axis, projected on the principal section PS.

θ_2: component angle of S', measured from the z axis, projected on the plane perpendicular to the principal section PS.

Ω_1: external tilt angle measured along the principal section PS.

Ω_2: external tilt angle measured along the plane perpendicular to the principal section PS.

ω_1: internal tilt angle measured along the principal section PS.

ω_2: internal tilt angle measured along the plane perpendicular to the principal section PS.

n_{mean}: mean refractive index.

PS′: principal section containing the optic axis OA and the direction of propagation S'.

θ'_1: component angle of S', measured from the z axis, projected on the principal section PS′.

θ'_2: component angle of S', measured from the z axis, projected on the plane perpendicular to the principal section PS′.

Ω'_1: external tilt angle measured along the principal section PS′.

Ω'_2: external tilt angle measured along the plane perpendicular to the principal section PS′.

ω'_1: internal tilt angle measured along the principal section PS′.

ω'_2: internal tilt angle measured along the plane perpendicular to the principal section PS′.

ψ'_1: component angle equal to $\theta'_1 + \omega'_1$ measured from the z axis along the principal section PS′.

δ_{0S}: relative phase difference measured down the direction of propagation S.

t_{eff}: effective thickness of the sample defined by the path length traveled by light within the sample.

E: electric field.

D: electric displacement.

H: magnetic field.

B: magnetic induction.

k: wavevector.

S: Poynting vector.

We are grateful to the Engineering and Physical Sciences Research Council for a grant enabling this work to be carried out. We also would like to thank Dr Neil Mancktelow for the Alpine quartzite samples used in the preferred orientation study.

References

Born, M. & Wolf, E. (1999). *Principles of Optics*. Cambridge University Press.

Deer, W. A., Howie, R. A. & Zussman, J. (1992). *The Rock-Forming Minerals*, 2nd ed. Harlow, UK: Longman.

Geday, M. A. & Glazer, A. M. (2002). *J. Appl. Cryst.* **35**, 185–190.

Geday, M. A., Kaminsky, W., Lewis, J. G. & Glazer, A. M. (2000). *J. Microsc.* **198**, 1–9.

Geday, M. A., Kreisel, J., Glazer, A. M. & Roleder, K. (2000). *J. Appl. Cryst.* **33**, 909–914.

Glazer, A. M., Lewis, J. G. & Kaminsky, W. (1996). *Proc. R. Soc. London Ser. A*, **452**, 2751–2765.

Hartshorne, N. H. & Stuart, A. (1964). *Practical Optical Crystallography*. London: Edward Arnold.

Hartshorne, N. H. & Stuart, A. (1970). *Crystals and the Polarizing Microscope*, 4th ed. London: Edward Arnold.

Heilbronner, R. (2000). *Optical Orientation Imaging*, in *Stress, Strain and Structure, a Volume in Honour of W. D. Means*, edited by M. W. Jessel & J. L. Urai, *J. Virtual Explorer*, **2**.

Hollingsworth, M. D. & Peterson, M. L. (2002). *Proc. NASA Microgravity Materials Science Conference*. Washington, DC: NASA.

Mancktelow, N. S. (1987). *Tectonophysics*, **135**, 133–153.

Owen, R. L. & Garman, E. (2005). *Acta Cryst.* D**61**, 130–140.

Petykiewicz, J. (1992). *Wave Optics*. Warsaw: Polish Scientific Publishers.

Shuvaeva, V. A., Glazer, A. M. & Zekria, D. (2005). *J. Phys. Condens. Matter*, **17**, 5709–5723.

Tixier, T., Heppenstall-Butler, M. & Terentjev, E. M. (2005). *Eur. Phys. J. E*, **18**, 417–423.

Wahlstrom, E. E. (1965). *Optical Crystallography*, 3rd ed. New York: John Wiley.

Wenk, H. R. & Van Houtte, P. (2004). *Inst. Phys. Publ.* **67**, 1367–1428.

Ye, C., Liu, S., Teng, X., Fang, Q. & Li, G. (2006). *Meas. Sci. Technol.* **17**, 436–440.